Stereology and Image Analysis. Ecs10 - Proceedings of the 10th European Congress of ISS,
(V.Capasso et al. Eds.), The MIRIAM Project Series, ESCULAPIO Pub. Co., Bologna, Italy, 2009

APPLICATIONS OF ANISOTROPIC IMAGE FILTERS FOR COMPUTING 2D AND 3D-FIBER ORIENTATIONS

OLIVER WIRJADI[1], KATJA SCHLADITZ[1], ALEXANDER RACK[2] AND THOMAS BREUEL[3]

[1]Image Processing Group, Fraunhofer ITWM, 67663 Kaiserslautern, Germany, [2]X-ray Imaging Group ID22, European Synchrotron Radiation Facility, 38043 Grenoble, France, [3]Computer Science Department, University of Kaiserslautern, 67663 Kaiserslautern, Germany
e-mail: wirjadi@itwm.fraunhofer.de

ABSTRACT

Fiber-reinforced materials such as glass and carbon fiber-reinforced polymers or ultra high performance concretes find an increasing number of applications *e.g.* in construction of bridges, automotive and aerospace engineering. Due to their matrix, such materials typically posses high compressive strengths while the fibers contribute tensile strength to the overall material properties. Measuring these fibers' orientation distribution in images obtained *e.g.* by micro-computed tomography (μCT) or scanning acoustic microscopy (SAM) enables an assessment of mechanical properties of a specimen. Unfortunately, image quality is often low, which complicates the segmentation of fibers in such images. We have recently proposed a method for computing fiber orientations directly from gray valued images. This method applies anisotropic Gaussian convolution filters to find the likely local orientation in each pixel. An efficient implementation of this filter operation in 2D and 3D is available. By accumulating the local orientations of foreground pixels in the second order orientation tensor, mean fiber orientations and information on the shape of the fiber orientation distribution can be computed. We here propose a novel sampling scheme for this method, evaluate its accuracy on simulated data and apply it to compute fiber orientations in a μCT-reconstruction of a carbon fiber-reinforced polymer.

Keywords: anisotropic image filter, fiber orientation, orientation space, fiber-reinforced polymer, CT.

INTRODUCTION

The fiber orientation distribution is an important factor influencing the properties of various fibrous materials. This has been shown to be true *e.g.* in bones (Martin and Boardman, 1993) as well as in ultra high performance concretes (Markovic, 2006). Examples from materials science include the work of Fu and Lauke (1996), who developed models for fiber lengths and orientations to study their effects on the tensile strength of fiber-reinforced polymers, and Hine and Duckett (2004), who investigated the effect of local orientations on stiffness and thermal expansion in glass fiber-reinforced materials.

Motivated by such results from the literature, we here focus on algorithms for computing the fiber orientation distribution in fiber-reinforced polymers, but the method may also be applicable to other materials.

The many proposed methods for analyzing fiber systems include various stereological approaches, *e.g.* (Clarke *et al.*, 1995; Lee *et al.*, 2003; Redon *et al.*, 1998). Kiderlen and Pfrang (2005) demonstrated how to compute the rose of directions, the direction distribution of the fibers' tangent vector in the typical fiber point, from fiber counts in oriented planar cuts. This requires them to segment fiber profiles in 2D-images. Given a segmentation of individual fibers in 3D-images obtained by μCT, the fibers' orientation, spatial distribution or shape are accessible. Therefore, various segmentation methods have been applied to fibers, *e.g.* (Aylward and Bullit, 2002; Donoser and Bischof, 2006; Yang and Lindquist, 2000). Either way, image segmentation is the performance limiting step.

Other approaches to measuring fiber orientations utilize gradient information. The first derivative is useful for edge detection and has been used to compute 2D-fiber orientation distributions (Gadala-Maria and Parsi, 1993). Second order derivatives, suitable to detect ridge-like structures such as fibers (Eberly *et al.*, 1994), can be applied either to an image's auto-correlation function (Napadow *et al.*, 2001), or directly to a grayscale image, *e.g.* (Daniels *et al.*, 2006; Frangi *et al.*, 1998; Sato *et al.*, 1997). The advantage of these gradient-based over segmentation-based methods is that they can detect subtle changes in an image's gray values, even when some segmentation algorithms may fail on that data.

Following this general idea, the present paper uses anisotropic Gaussian convolution filters in 2D and 3D to compute fiber orientation distributions. Similar approaches such as (Chen *et al.*, 2000) or (Faas and van Vliet, 2003) apply such concepts for segmentation. In contrast, we show how the filter results directly lead to an algorithm for analyzing fiber orientation distributions, without segmenting individual fibers. Our easily implementable approach to fiber orientation measurement will be shown to deliver accurate results. Results from the proposed method are different forms of orientation measures such as discrete distributions on the sphere, orientation tensors or mean fiber directions. We here extend our previous work (Robb *et al.*, 2007) by a novel sampling method, numerical evaluations and a new application example demonstrating the applicability of our method to carbon fiber-reinforced polymers.

METHOD

Anisotropic convolution filters are useful for adaptive image smoothing by aligning them to local image structures, see *e.g.* (Lee *et al.*, 2006). They can, on the other hand, also be used to detect image structures, which is done in this paper. Different types of filters could be used for this purpose, and we will use d-dimensional anisotropic Gaussian filters, for they possess an intuitive parameterization, see below, and are implementable with linear runtime complexity (Lampert and Wirjadi, 2006). The Gaussian convolution kernel is given by

$$g(\mathbf{x}) = \frac{1}{(2\pi)^{d/2}|\Sigma|^{1/2}} \exp\left(-\frac{1}{2}\mathbf{x}^t\Sigma^{-1}\mathbf{x}\right). \quad (1)$$

Here, Σ denotes the $d \times d$ symmetric positive definite covariance matrix, and $|\Sigma|$ its determinant. The $\frac{d(d+1)}{2}$ degrees of freedom of Σ encode the filter's shape. Its Eigen decomposition,

$$\Sigma = (\mathbf{v}_1, \ldots, \mathbf{v}_d) \begin{pmatrix} s_1 & & \\ & \ddots & \\ & & s_d \end{pmatrix} (\mathbf{v}_1, \ldots, \mathbf{v}_d)^t, \quad (2)$$

into Eigen vectors $\mathbf{v}_i \in \mathbb{R}^d$ and d Eigen values $s_i \in \mathbb{R}$ is useful for interpreting this encoding. The $\mathbf{v}_i$ describe the orthogonal filter axes and the s_i the size of the filter kernel in those directions. For detecting fibers in 2D, we may choose $s_2 > s_1$, resulting in an elliptic filter shape that fits well to fibers with diameter $2s_1$. In 3D, the filter has three orthogonal axis directions ($\mathbf{v}_1$, $\mathbf{v}_2$ and $\mathbf{v}_3$), and three filter size parameters (s_1, s_2 and s_3) in the corresponding directions. By choosing parameters $s_3 > s_2 = s_1$, a filter with the shape of a prolate spheroid results, which fits well to fibers with circular profiles. With these parameterizations, the response of the filter g at a pixel $\mathbf{x}$ is expected to be maximized when the filter's direction $\mathbf{v}_d$ is aligned to a fiber in that point, both in 2D ($d = 2$) and 3D ($d = 3$).

Let $g_\mathbf{v}$ denote an anisotropic Gaussian convolution kernel with $\mathbf{v}_d = \mathbf{v}$ and let f be a d-dimensional image. Following the reasoning above, define the reduced orientation space $O(\mathbf{x})$ as

$$O(\mathbf{x}) = (r(\mathbf{x}), \mathbf{v}(\mathbf{x})), \quad (3)$$

where $r(\mathbf{x}) = \max_\mathbf{v}[g_\mathbf{v} * f](\mathbf{x})$, $\mathbf{v}(\mathbf{x}) = \operatorname{argmax}_\mathbf{v}[g_\mathbf{v} * f](\mathbf{x})$, and $*$ denotes convolution. We refer to $O(\mathbf{x})$ as a *reduced* orientation space as it contains the direction of maximal filter response $r(\mathbf{x})$, only. $\mathbf{v}(\mathbf{x})$ represents the most likely local orientation in a point $\mathbf{x}$ under the model g. To compute $O(\mathbf{x})$, we search over a set of sampling directions, see below. The filter size parameters, on the other hand, are chosen relative to the fiber radius r, which is assumed to be known and constant throughout the image: Set $s_d = 2r$ and $s_1 = r$ or $s_1 = s_2 = r$ in 2D or 3D, respectively.

SAMPLING DIRECTIONS

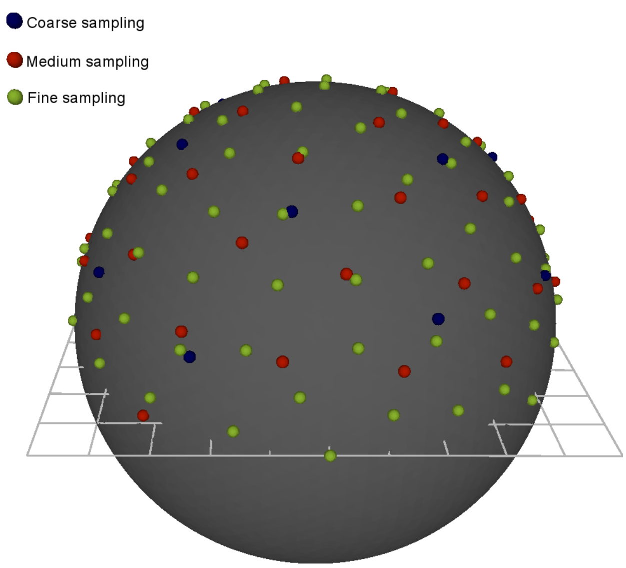

Fig. 1. *Three sets of sampling points used for computing the reduced orientation space $O(\mathbf{x})$ in 3D.*

The procedure described above filters the image f in n directions $\{\mathbf{v}^i\}_{i=1,\ldots,n}$. To avoid a bias in the results, it is important to choose these n directions uniformly placed on the half-sphere. In 2D, this is easily achieved by dividing the half-circle in n equiangular steps. In 3D, however, choosing n points that partition the hemisphere uniformly is not trivial. A number of methods for the unit ball have been proposed, see *e.g.* (Saff and Kuijlaars, 1997). Here, we follow a numerical method proposed by Fliege and Maier (1999), who gave an optimization algorithm for distributing n points on the unit sphere S^2. We modified their original algorithm by optimizing a set of $2n$ points on S^2, which contain the mirror point $-\mathbf{v}$ for each vector $\mathbf{v}$. This procedure results in a set of points placed equally (except for the sign) on the upper and lower hemisphere. Only the vectors on the upper hemisphere (positive sign in their third component) will be used, thus yielding suitable sampling directions.

This was performed for $n = 18, 50, 98$, resulting in three orientation space resolution levels, which will be referred to as *coarse*, *medium* and *fine* sampling, respectively (Fig. 1).

ORIENTATION TENSORS

The reduced orientation space of an image is not useful on its own. This section therefore introduces methods for averaging and summarizing the orientation information contained in $O(\mathbf{x})$.

Histograms of the local orientations $\mathbf{v}(\mathbf{x})$ can be graphically mapped onto the circle or sphere to visualize the fiber orientation distribution in an image f, see (Robb *et al.*, 2007). For quantitiative interpretations of $O(\mathbf{x})$, we use orientation tensors (Tucker and Advani, 1994). They are frequently used for simplifying the computation of directional averages when simulating mechanical properties of fibrous materials, see *e.g.* (Camacho *et al.*, 1990; Kim and Song, 1997). Let p be a density defined on the sphere S^{d-1} with $p(\mathbf{v}) = p(-\mathbf{v})$. Orientation tensors are then defined as the moments of the distribution p. The second order orientation tensor a_{ij},

$$a_{ij} = \int_{S^{d-1}} v_i v_j p(\mathbf{v}) d\mathbf{v}, \tag{4}$$

is $\mathbf{v}$'s correlation matrix and therefore represents an ellipsoidal approximation of p's shape. Here, v_i denotes the i'th component of $\mathbf{v}$, and $i, j = 1, \ldots, d$.

The use of a_{ij} from an image analysis perspective is twofold. It comprises a convenient method for averaging directional information over images or image areas, see below, and it can directly be used in subsequent simulation studies using methods such as those described in the references given above. Therefore, a number of authors have used a_{ij} to describe the orientation of fibers in images. Among those are approaches for computing a_{ij} using stereological methods (Eberhardt and Clarke, 2001; Harrigan and Mann, 1984; Lee *et al.*, 2003), and by integrating over the responses of quadrature filters instead of p as in Eq. (4) (Knutsson, 1989).

To compute a_{ij} from the reduced Gaussian orientation space $O(\mathbf{x})$, we use sample averages over all pixels belonging to the fiber system B. B is identified by a global gray value threshold t_0,

$$B = \{\mathbf{x} | f(\mathbf{x}) > t_0\}, \tag{5}$$

assuming that fibers appear with larger gray values than the background. In practical experiments setting t_0 to 10% above Otsu's threshold (Otsu, 1979) was sufficient for all datasets tried. To choose a high threshold t_0 is appropriate here as it eliminates pixels close to fiber edges, where orientation estimates are least stable. In a window W, a_{ij} is then estimated by

$$T_W := \frac{1}{|W \cap B|} \sum_{\mathbf{x} \in W \cap B} \mathbf{v}(\mathbf{x}) \mathbf{v}^t(\mathbf{x}), \tag{6}$$

which we call the sample second order orientation tensor T_W. See (Fisher *et al.*, 1987) for how to compute the mean fiber orientation and other shape measures of the fiber orientation distribution p from T_W,

For averaging over $W \cap B$ to yield correct sample orientation tensors, a few conditions have to be met. In stochastic geometry, random fiber processes are described by sets of finite smooth curves. Their orientations are characterized by the tangential vectors of these curves, which posses distributions that are random measures on the circle or sphere. For a rigorous definition, see (Stoyan *et al.*, 1995). Then, for a system of non-overlapping fibers, the distribution of the tangential direction vectors, $p(\mathbf{v})$, is a length-weighted distribution, since each fiber contributes proportionally to its length to the overall probability mass. Under the assumption made above that all fibers have equal diameter $2r$, this is also true for the sample mean over $\mathbf{v}\mathbf{v}^t$ in (6), as the number of pixels that a single fiber contributes to B is then proportional to its length.

A potential problem in evaluating (6) is the edge treatment. When observing stochastic processes in finite areas W, realizations of large objects, in the present case long fibers, have a higher probability of intersecting the boundary than small objects. This can lead to a bias in the estimated quantity. Different methods to avoid this problem have been proposed, see *e.g.* (Baddeley and Jensen, 2004) for an overview. These methods, however, all rely on individually segmented objects being available.

As the present paper describes a method for orientation estimation that does not rely on the segmentation of fibers, there is no immediate remedy for the edge correction problem. Therefore, when estimating T_W using (6), one has to either choose a sufficiently large observation window W, or the orientation of an individual fiber must be independent of its length.

RESULTS

Next, we will test the proposed method with respect to accuracy and runtime requirements. All results in this section were performed on artificially generated 2D and 3D data.

ACCURACY

To measure the accuracy of local orientations, we used an overlapping Markov fiber process. Starting with a random pixel and direction, a new direction vector is drawn from a von Mises-Fisher distribution (Fisher *et al.*, 1987) with respect to the previous direction (Fig. 2(a)). The next point is then generated by moving one unit step in this new direction. The von Mises-Fisher distribution has a scalar spread parameter, κ, which is used here to control the curvature of the generated fibers.

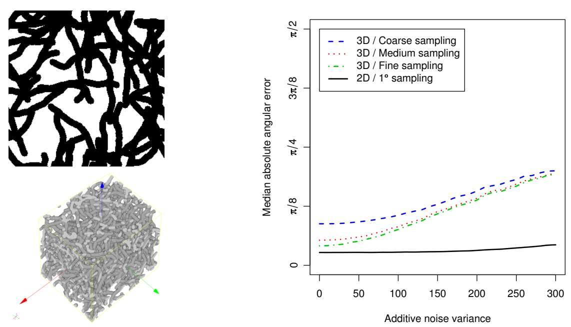

(a) Simulated test data. (b) Accuracy on test data.

Fig. 2. *Median angular difference between the true and estimated tangent fiber direction along the central fiber path of simulated overlapping fibers. Local orientation estimates are more accurate in 2D than in 3D.*

With this setup, we generated images with random overlapping fiber systems and known tangent directions $\mathbf{v}^*(\mathbf{x})$ in every fiber point $\mathbf{x} \in B$. To measure the accuracy of the proposed method, the inner product between true and estimated directions, $\arccos \mathbf{v}^t \mathbf{v}^*$, along the fiber paths was used (Fig. 2). The proposed method is robust to some degree of additive noise. The influences of choosing a resolution level are clearly visibly, but these differences diminish as the amount of noise increases. In general, the proposed method is more precise and more robust to noise in 2D than in 3D. We attribute these differences to the angular sampling, which is much finer in 2D (1°) than in 3D (13.8° on average for “fine” sampling).

RUNTIME

Implementation of the anisotropic Gaussian convolution has linear time complexity in the number of pixels, both in 2D and 3D (Lampert and Wirjadi, 2006). Given the choice of a resolution level, computation of the reduced Gaussian orientation space in Eq. (3) requires a fixed number of such filter operations. Thus, the overall time complexity remains linear in the number of pixels.

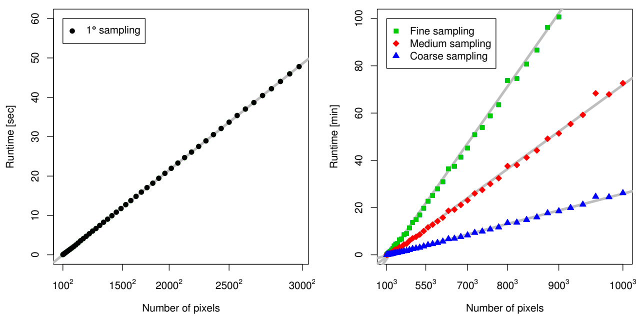

(a) 2D (b) 3D

Fig. 3. *Experiments demonstrate the linear runtime depending on the number of pixels of the proposed method. All measurements shown here were performed on a single core of an Intel Xeon 2.5GHz CPU (E5420) running GNU/Linux.*

To verify whether this statement holds in practice, we measured the runtime of our implementation of Eq. (3) on a single processor (Fig. 3). The runtime indeed depends linearly on the number of pixels. With overall processing times in the range of one minute and one hour for common 2D and 3D image data sizes, respectively, we judge the computational burden of the method proposed in this paper to be tractable.

APPLICATION: CARBON FIBER-REINFORCED POLYMER

Among modern composite materials, carbon fiber-reinforced polymers (CRP) are gaining importance in light-weight applications such as fuselages of modern aircrafts. Imaging and analysis of the fiber systems of CRPs is very challenging due to small fiber size (diameters well below 10μm), high fiber density (fiber volume fraction above 60% for the CRP processed here) and the low material contrast between carbon and polymers. Synchrotron μCT can image the full three dimensional structure at spatial resolutions in the range of 1μm in specimen with side lengths up to about 1.5mm. The combination of a good signal to noise ratio and X-ray phase contrast techniques delivers volume images which allow one to visually identify single fibers, *cf.* Fig. 5. Nevertheless, the small inter-fiber distances, partially below the spatial resolution of the imaging system and the inhomogeneous phase contrast (in principle an edge enhancement), make accurate segmentation of individual fibers difficult if not impossible.

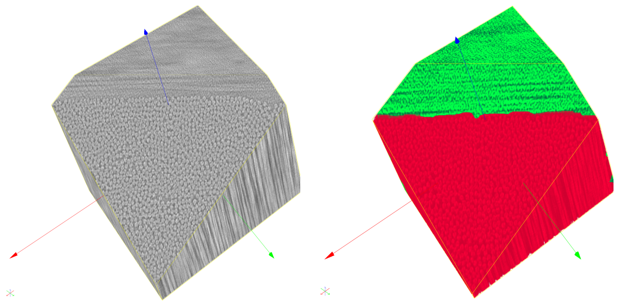

(a) Visualization of a part (512^3) of a μCT-reconstruction of a CRP.

(b) Segmentation of two differently oriented fiber layers by their local orientations.

Fig. 4. *Application of the proposed method to a synchrotron μCT-reconstruction of a carbon fiber-reinforced polymer (sample by R. Stößel, EADS).*

The analysis method proposed in this paper, on the other hand, is suitable for analyzing such data as it is capable of detecting anisotropies in the image texture. To demonstrate this, we applied our method to a μCT-image of a CRP acquired at ESRF Grenoble with a spatial resolution of 0.7μm. The carbon fibers have a diameter of about 5μm, therefore we set $s_1 = s_2 = 4$ pixels and $s_3 = 8$ pixels and computed $O(\mathbf{x})$ by sampling $\mathbf{v}_3$ along the 98 directions in the “fine” resolution set shown in Fig. 1.

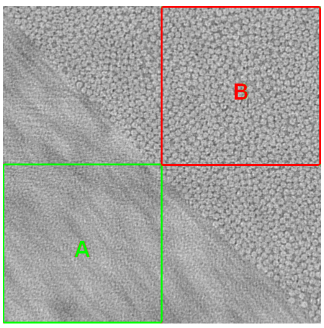

$$T_B = \begin{pmatrix} .24 & .09 & .05 \\ .10 & .26 & .07 \\ .05 & .07 & .50 \end{pmatrix}$$

$$T_A = \begin{pmatrix} .35 & .09 & .04 \\ .09 & .38 & .06 \\ .05 & .06 & .26 \end{pmatrix}$$

Fig. 5. *The orientation tensors computed in two distinct areas of the carbon fiber-reinforced polymer sample. The differently oriented fiber systems in the two areas are clearly picked up by our method.*

The resulting local orientations clearly differentiate between the differently oriented fiber layers in this specimen, which can be seen in Fig. 4, where we used the local orientations $\mathbf{v}(\mathbf{x})$ from $O(\mathbf{x})$ to segment the total volume into two areas. Such a segmentation result could be used in a subsequent analysis step to provide layer-specific information such as volume densities or mean orientations.

To demonstrate the latter, we further evaluated the sample second order orientation tensor from Eq. (6) in these two distinct fiber layers (Fig. 5). The resulting tensors reveal a z-axis parallel fiber orientation area B (shown in red), which can be seen from the dominating third element of T_B's matrix diagonal. Fiber area A (shown in green), on the other hand, contains fibers with orientations largely in the xy-plane, as indicated by two about equally large dominating entries in the first two elements on the matrix diagonal of T_A.

DISCUSSION

We described a method for computing local fiber orientations and their distributions from 2D and 3D images. For fiber reinforced-polymers, where fibers typically posses constant radii, sample averages of the resulting orientation vectors yield an estimate of the orientation tensor. Furthermore, the method was demonstrated to be suitable for analyzing μCT images of a carbon fiber-reinforced polymer. Anisotropic image filters are valuable tools for processing image data of the microstructure of fibrous materials, especially when image resolution or quality are insufficient for segmentation of individual fibers.

ACKNOWLEDGMENT

This work was supported in part by $(CM)^2$ – Center for Mathematical + Computational Modelling. We are grateful to R. Stößel for providing the CRP sample.

REFERENCES

Aylward S, Bullit E (2002). Initialization, noise, singularities, and scale in height ridge traversal for tubular object centerline extraction. IEEE Trans Medical Imaging 21:61–75.

Baddeley A, Jensen EV (2004). Stereology for Statisticians. Monographs on Statistics and Applied Probability. Boca Raton, FL, USA: Chapman & Hall/CRC.

Camacho C, Tucker C, Yalvaç S, McGee R (1990). Stiffness and thermal expansion predictions for hybrid short fiber composites. Polymer Composites 11:229–39.

Chen J, Sato Y, Tamura S (2000). Orientation space filtering for multiple orientation line segmentation. IEEE Trans Pattern Analysis and Machine Intelligence 22:417–29.

Clarke A, Archenhold G, Davidson N (1995). A novel technique for determining the 3D spatial distribution of glass fibres in polymer composites. Composites Science and Technology 55:75–91.

Daniels F, ter Haar Romeny B, Rubbens M, van Assen H (2006). Quantification of collagen orientation in 3D engineered tissue. In: Proc. Kuala Lumpur Int. Conf. Biomedical Engineering.

Donoser M, Bischof H (2006). 3D segmentation by maximally stable volumes (MSVs). In: Proc. Int. Conf. Pattern Recognition.

Eberhardt C, Clarke A (2001). Fibre-orientation measurements in short-glass-fibre composites. Part I: automated, high-angular-resolution measurement by confocal microscopy. Composites Science and Technology 61:1389–400.

Eberly D, Gardner R, Morse B, Pizer S, Scharlach C (1994). Ridges for image analysis. J Mathematical Imaging and Vision 4:353–73.

Faas F, van Vliet L (2003). 3D-orientation space; filters and sampling. In: Proc. Scandinavian Conf. Image Analysis.

Fisher N, Lewis T, Embleton B (1987). Statistical Analysis of Spherical Data. Cambridge, UK: Cambridge University Press.

Fliege J, Maier U (1999). The distribution of points on the sphere and corresponding cubature formulae. IMA J Numerical Analysis 19:317–34.

Frangi A, Niessen W, Vincken K, Viergever M (1998). Multiscale vessel enhancement filtering. In: Proc. Medical Image Computing and Computer-Assisted Intervention.

Fu S, Lauke B (1996). Effects of fiber length and fiber orientation distributions on the tensile strength of short-fiber-reinforced polymers. Composites Science and Technology 56:1179–90.

Gadala-Maria F, Parsi F (1993). Measurement of fiber orientation in short-fiber composites using digital image processing. Polymer Composites 14:126–31.

Harrigan T, Mann R (1984). Characterization of microstructural anisotropy in orthotropic materials using a second rank tensor. J Materials Science 19:761–7.

Hine P, Duckett RA (2004). Fiber orientation structures and mechanical properties of injection molded short glass fiber reinforced ribbed plates. Polymer Composites 25:237–54.

Kiderlen M, Pfrang A (2005). Algorithms to estimate the rose of directions of a spatial fibre system. J Microscopy 219:50–60.

Kim J, Song J (1997). Rheological properties and fiber orientations of short fiber-reinforced plastics. J Rheology 41:1061–85.

Knutsson H (1989). Representing local structure using tensors. In: Proc. Scandinavian Conf. Image Analysis.

Lampert C, Wirjadi O (2006). An optimal non-orthogonal separation of the anisotropic Gaussian convolution filter. IEEE Trans Image Processing 15:3501–13.

Lee J, Chung M, Alexander A (2006). Evaluation of anisotropic filters for diffusion tensor imaging. In: Proc. 3rd IEEE Int. Symp. Biomedical Imaging.

Lee K, Lee S, Chung K, Kang T, Youn J (2003). Measurement and numerical simulation of three-dimensional fiber orientation states in injection-molded short-fiber-reinforced plastics. J Applied Polymer Science 88:500–9.

Markovic I (2006). High-Performance Hybrid-Fibre Concrete: Development and Utilisation. Amsterdam, NL: IOS Press.

Martin R, Boardman D (1993). The effects of collagen fiber orientation, porosity, density, and mineralization on bovine cortical bone bending properties. J Biomechanics 26:1047–54.

Napadow V, Chen Q, Mai V, So P, R JG (2001). Quantitative analysis of three-dimensional-resolved fiber architecture in heterogeneous skeletal muscle tissue using NMR and optical imaging methods. Biophysical Journal 80:2968–75.

Otsu N (1979). A threshold selection method from grey-level histograms. IEEE Trans Systems Man and Cybernetics 9:62–6.

Redon C, Chermant L, Chermant J, Coster M (1998). Assessment of fibre orientation in reinforced concrete using fourier image tansform. J Microscopy 191:258–65.

Robb K, Wirjadi O, Schladitz K (2007). Fiber orientation estimation from 3D image data: Practical algorithms, visualization, and interpretation. In: Proc. Int. Conf. Hybrid Intelligent Systems.

Saff E, Kuijlaars A (1997). Distributing many points on a sphere. The Mathematical Intelligencer 19:5–11.

Sato Y, Nakajima S, Atsumi H, Koller T, Gerig G, Yoshida S, Kikinis R (1997). 3D multi-scale line filter for segmentation and visualization of curvilinear structures in medical images. In: Proc. Joint Conf. Computer Vision, Virtual Reality and Robotics in Medicine and Medial Robotics and Computer-Assisted Surgery.

Stoyan D, Kendall W, Mecke J (1995). Stochastic Geometry and its Applications. Chichester, UK: John Wiley & Sons, 2nd ed.

Tucker C, Advani S (1994). Processing short-fiber systems. In: Advani S, ed., Flow and Rheology in Polymer Composites Manufacturing, Composite Materials. Amsterdam, NL: Elsevier, 147–202.

Yang H, Lindquist W (2000). Three-dimensional image analysis of fibrous materials. In: Proc. SPIE Applications of Digital Image Processing XXIII, vol. 4115.